



Research Article

Monitoring Rice Phenological Stages Using Temporal Sentinel-1 SAR Data

L. HARIKA¹, MAMTA KUMARI^{2*}, T.L. NEELIMA¹, ABHISHEK CHAKRABORTY²
AND K. AVIL KUMAR¹

¹Water Technology Centre, PJTSAU, Rajendranagar, Hyderabad-500030, Telangana

²Agricultural Sciences & Applications Group, RS & GIS – Applications Area, National Remote Sensing Centre, Indian Space Research Organization, Hyderabad, Telangana

ABSTRACT

Rice is the principal food crop mostly grown during *kharif* season in India. The persistent cloud cover during *kharif* season makes the rice phenology monitoring complicated using optical remote sensing. In this scenario, microwave data has been shown to be a reliable form to acquire cloud free data. This study utilised the temporal Sentinel-1 SAR and Sentinel-2 optical data for the paddy phenology monitoring for the *kharif* season in the Nizamabad district, Telangana, India, in the year 2021. Temporal VH backscatter and NDVI profiles could characterise the staggered transplanting periods of paddy. All the SAR based observables such as, VH backscatter, VV backscatter, RVI, ratio (VH/VV) showed sensitivity to paddy growth stages however, VV-VH and VV+VH backscattering were also sensitive to some of the stages. Among all VH, VH/VV, and RVI backscattering power combined could be utilised to identify the paddy phenological growth stages with an accuracy of 68.42%.

Key words: Paddy, SAR, Crop phenology, Temporal profile, NDVI

Introduction

Global population rise is increasing the demand for agriculture, triggering the need for precise crop monitoring for adequate production. Rice is a staple food for almost 4 billion people globally and contributes to 19% of the daily human energy supply, which ranked first among the cereals (Elert, 2014). It provides 15% of per capita protein and 21% of global human per capita energy (United Nations, 2017). Rice production is been increasing from 1994 till 2019 (FAOSTAT, 2021), with the production of 148.30 MT in China, followed by 120.00 MT in India for 2020-2021 (USDA, 2022). Timely and efficient rice mapping and phenology monitoring will help in sustainable and precision farming benefiting food

security. Besides, the paddy crop plays a very considerable role in impacting climate change and water resource use (Dong and Xiao, 2016). Phenological development information is a key for crop monitoring as it depicts the actual state of the crop.

Remote sensing technology has been widely used in temporal profile analysis of crop. Synoptic coverage through satellite remote sensing provides an efficient approach to monitor and map the rice crop. Moderate Resolution Imaging Spectroradiometer (MODIS) data with a high temporal resolution have been widely used for many years (De Castro *et al.*, 2018; Onojeghuo *et al.*, 2018). Although it can identify paddy fields, its coarse spatial resolution (500 m) makes its use limited or can be used in combination with fine spatial resolution data (Pipia *et al.*, 2022; Sisheber *et al.*, 2022; Li *et al.*,

*Corresponding author,
Email: mamta9507@gmail.com

2021). Recently launched Sentinel-2 (S-2) which has two satellite constellations offers high spatial (10 m) and temporal resolution (5 day) has been explored for the crop phenology monitoring in several studies (Htitiou *et al.*, 2022; Amin *et al.*, 2022). However, as the majority of rice cultivation happens in *kharif*, dense cloud cover hinders the optical satellite data acquisition capability. Synthetic Aperture Radar (SAR) systems operate in the microwave range (1mm to 1m) of EM spectrum with all-weather data acquisition capability, and due to its longer wavelength can penetrate the clouds with negligible attenuation. Besides, SAR backscatter response depends on the dielectric and geometric properties of the targets.

The potential of Synthetic Aperture Radar (SAR) data for rice crop mapping and monitoring has been demonstrated by a number of investigators (Le Toan *et al.*, 1997; Shao *et al.*, 2001; Chakraborty *et al.*, 2005; Bouvet *et al.*, 2009). Multi-temporal SAR data is suitable for crop monitoring and condition assessment as variations in crop growth can be observed and characterized using SAR observables (Wu *et al.*, 2010; Moran *et al.*, 2011). The utility of SAR data for phenology monitoring of rice had been first shown by Lopez *et al.* (2011), for the identification of rice phenology using TerraSAR-X

dual-pol SAR observables according to BBCH (Biologische Bundesanstalt, Bundessortenamt und Chemische Industrie) scale (Meier, 1997) and later it was extended to quad-polarimetric C-band SAR data (Lopez *et al.*, 2013). Sentinel-1 (S-1) launched by European Space Agency (ESA), is a new SAR data source with a high spatiotemporal resolution and is explored for crop monitoring and mapping (Harfenmeister *et al.*, 2021; Low *et al.*, 2021; Pandit *et al.*, 2021; Wanget *et al.*, 2022; Wang *et al.*, 2022; Zhao *et al.*, 2022). Although rice phenology monitoring is well studied globally, a limited work has been conducted in India. Keeping all the above points in view, this study aims to assess the potential of Sentinel-1 and Sentinel-2 data to analyze the temporal behavior of SAR backscatter and NDVI at different rice crop phenological growth stages. In this study, a relatively simple approach is applied from Sentinel-1 SAR observables for phenology estimation of rice crop.

Study area

The present study was conducted in the Nizamabad district, Telangana, which is located between latitude of 18°41' North and longitude of 78°6' East (Fig. 1), covering an area of 4288 km², with a mean elevation of 395 meters above mean

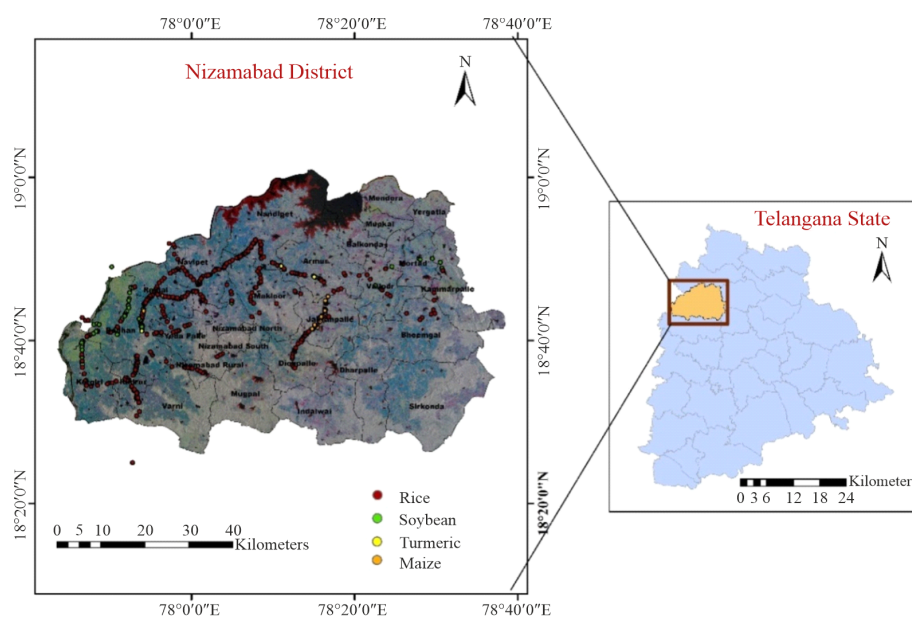


Fig. 1. Study area (Nizamabad district of Telangana state, India) along with field visit ground truth points superimposed on color composite of 3 dates of VH backscatter data (red-12th July, green-17th August, blue-28th October 2021)

sea level. Average rainfall in the district is 1024.4 mm, usually received during the South-west monsoon from July to October. Soils of Nizamabad district varies from black soils to chalka. The farming system comprises of mostly irrigated cropping system (single, inter and multiple cropping) which include paddy, maize, red gram, jowar, intercropping of soybean with red-gram and turmeric with red gram. The rice planting in the study area was very staggered. The rice crop that is transplanted in the

June was considered as early rice, July as normal rice, and August as late rice. The two major paddy varieties grown were MTU 1010 (Cottondora sannalu) of 120 days duration and BPT 5204 (Samba mahsuri) of 145 days duration. Other crops like cotton, sugarcane, groundnut and sesamum were scattered across a small region.

These five growth periods (Fig. 2) for rice in study area are Transplanting (01 Jun–15 Aug), Early







| Paddy growth stages | | |
|-------------------------|---|--|
| Principal crop period | Stage | Photograph |
| Transplanting | Transplanted |  |
| Early vegetative | Leaf development Tillering |  |
| Late vegetative | Stem elongation Booting Maximum tillering |  |
| Reproductive | Heading Flowering Development of grain |   |
| Maturity | Ripening Senescence |  |

Fig. 2. Growth phases of paddy

| Month | June | | | July | | | August | | | September | | | October | | | November | | | |
|-------------|-------------|----|-----|-------------|----|-----|-------------|----|-----|--------------|----|-----|--------------|----|-----|--------------|----|-----|--|
| Ten days | I | II | III | I | II | III | I | II | III | I | II | III | I | II | III | I | II | III | |
| Early rice | Olive Green | | | Light Green | | | Dark Green | | | Light Orange | | | Dark Orange | | | | | | |
| Normal rice | | | | Olive Green | | | Light Green | | | Dark Green | | | Light Orange | | | Dark Orange | | | |
| Late rice | | | | | | | Olive Green | | | Light Green | | | Dark Green | | | Light Orange | | | |

Fig. 3. Rice crop calendar in Nizamabad district from June to November, showing the early, normal, and late rice patterns. I, II, and III represents ten days phase of a month (Color coding: olive green- transplanted stage, light green- early vegetative stage, dark green- late vegetative stage, light orange - reproductive stage, dark orange - maturity)

vegetative (01 Jul–15 Sep), Late vegetative (01 Aug - 07 Oct), Reproductive (15 Aug - 30 Oct), and Maturity (25 Sep - 30 Nov). The exact dates of each period vary with the rice type, and weather conditions during the growth cycle of the rice crop (Fig. 3). The rice calendar described here illustrates typical rice growth behaviour in the Nizamabad district and will vary with the geographic location, ecological conditions, local climate, variety of rice, and especially the transplanting date.

Data collection

Satellite data

The current study has used Sentinel-1 SAR data and Sentinel-2 Optical data with a fine spatial resolution and frequent revisit interval to extract temporal profiles of paddy. The two identical polar-orbiting satellites Sentinel-1A and Sentinel-1B (dual-polarised VV, VH) operated by European Space Agency's, Copernicus program provide the SAR data. Sentinel-2A and 2B operated by ESA provide optical data. In this study, a total of fifteen Sentinel-1 images and twelve Sentinel-2 images from June to November of 2021 are used.

The backscatter values and the derived observables were studied using the cross-polarized (VH) and co-polarized (VV) SAR data. Maximum value composite (MVC) images of Normalised Difference Vegetation (NDVI) generated at fortnight (FN) intervals were studied.

Ground reference data

The extensive ground truth data was collected using mobile-based app and by interview of local farmers (Fig.1). Field observations include crop type, crop phenology and crop health in the study area. A total number of 546 field points distributed across the entire study area were collected. Field data includes 477 points under paddy category and remaining 69 under other crop classes. The field point locations were selected based on crop type, size of field, and accessibility. We applied an agricultural mask on SAR and NDVI images to restrict the study to the agricultural area of Nizamabad district.

Methodology

Pre-processing of data

We used Google Earth Engine (GEE) platform to download and pre-process the S1 and S2 data for fast and efficient implementation of the steps. In this work, all the required S-1 and S-2 images for the Nizamabad district were retrieved from the (COPERNICUS/S1_GRD) and (COPERNICUS/S2) image collection, respectively, available in GEE. The data was pre-processed through several steps in GEE. The pre-processing steps for Sentinel-1 include: a) Radiometric calibration, b) Thermal noise removal, c) Orthorectification (Range Doppler Terrain Correction algorithm); d) Conversion of logarithmic backscatter (dB) to linear backscatter values; e) Application of 7×7 refined Lee filter to reduce speckle noise; and f) Conversion of speckle-reduced

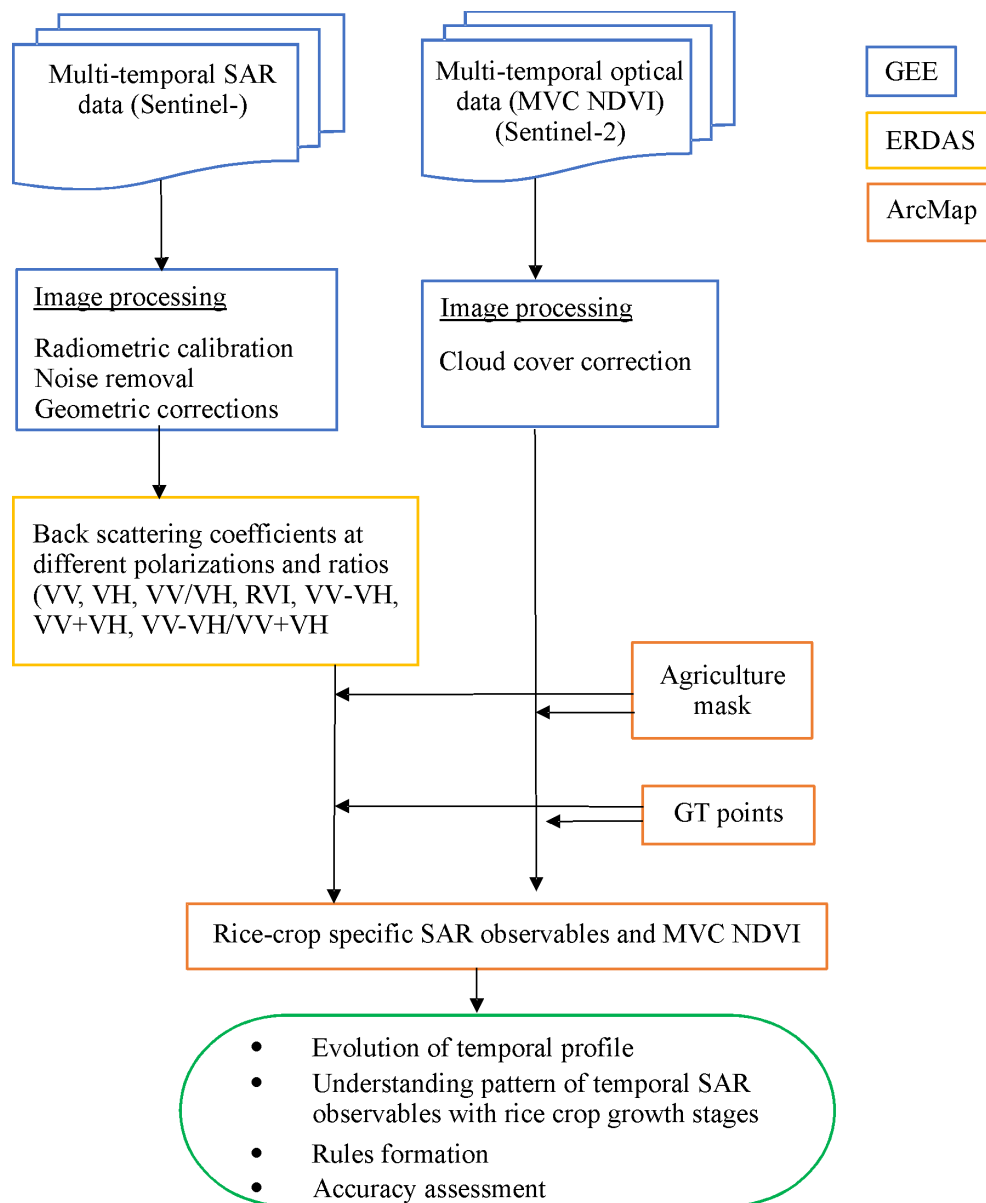


Fig. 4. Schematic diagram representing methodology

linear backscatter values to logarithmic backscatter values. The Sentinel-2 optical images processed in GEE through following steps: a) Normalised difference vegetation index (NDVI) computation; b) Maximum value composite (MVC) images generation at fortnight-interval using NDVI data; and c) Cloud masking.

Generation of SAR observables and NDVI

The SAR based observables were generated using different combinations of backscatter in VH

and VV polarisation. The SAR based observables used in the study are listed in Table 1.

Normalized Difference Vegetation Index (NDVI)

NDVI is one of the most widely used vegetation indices. The NDVI values ranges between +1.0 to -1.0. This spectral index was calculated from the red (band 4) and near infrared (NIR) (band 8) spectral bands of S-2 images.

Table1. SAR based observables

| S.No. | SAR observables | Derivation |
|-------|------------------------------|--|
| 1 | VV | VV co-polarised backscatter coefficient (σ^0 dB) |
| 2 | VH | VH cross-polarised backscatter coefficient (σ^0 dB) |
| 3 | VH/VV | Ratio of cross-polarised backscatter coefficient and co-polarised backscatter coefficient |
| 4 | VV-VH | Subtraction of co-polarised backscatter coefficient and cross-polarised backscatter coefficient |
| 5 | VV+VH | Sum of co-polarised backscatter coefficient and cross-polarised backscatter coefficient |
| 6 | VV-VH/VV+VH | Normalised ratio of (VV-VH) and (VV+VH) |
| 7 | Radar Vegetation Index (RVI) | $RVI = \frac{4 \sigma_{VH}^0}{\sigma_{VV}^0 + \sigma_{VH}^0}$ Where σ_{VV}^0 is co-polarised backscattering coefficient and σ_{VH}^0 is cross-polarised backscattering coefficient |

NDVI = NIR-R/ NIR+R

NIR = reflectance in near infrared band, R = reflectance in red band

Results and Discussion

Temporal evolution of SAR VH-backscatter and NDVI of paddy

The phenology-specific temporal variations of the NDVI was analysed to understand its correlation with growth stages of rice.

For the early rice (Fig. 5a), the NDVI value starts increasing from 2st FN of June (transplanting) and reaches to the maximum value of 0.7 during the late vegetative stage in 2nd FN of August. Later, it starts decreasing in as the crop reaches senescence (Hisham *et al.*, 2022; Ali *et al.*, 2021; Li *et al.*, 2014). There was a sudden dip in the NDVI value (0.2) in 1st FN of September due to heavy rainfall and cloudiness. Optical data could not penetrate the cloud so led to the loss of information. The normal rice (Fig. 5b) which was transplanted (0.1) in 1st FN of July, reached its maximum value of 0.8 in 1st FN of August and declined towards maturity (0.2). The dip was observed in 2nd FN of September due to cloudiness. For the late rice (Fig. 5c), the NDVI value increased from 1st FN of August (0.2); reached to the maximum value of 0.6 during the late vegetative stage in 1st FN of October; and later decreased in 2nd FN of

November at the maturity stage (0.3). As NDVI profiles were affected by cloud, SAR data which has the ability to penetrate through clouds has an advantage over optical data to analyse the rice phenology.

The temporal VH backscatter graph (Fig. 6) represented the different phenological growth stages of rice. The temporal variation of VH backscatter showed five distinct growth periods corresponding to different scattering mechanisms.

The difference in backscattering power in each period is resultant of difference in scattering mechanisms that emanated from the change in the geometric, structural, and dielectric properties of paddy crop during its growth cycle.

Temporal VH backscatter graph showed a substantial increase from -24 dB during transplanting to -15 dB during late vegetative stage, for early rice (Fig. 6a). The normal rice (Fig. 6b) showed a transplanting dip with a constant rise towards the late vegetative stage. Late rice also showed similar pattern (Fig. 6c). There was continuous decline in backscatter from reproductive to maturity stage. Hence, the rice phenological growth stages were distinguished based on the examination of the patterns of backscattering intensity in each period. Before transplanting, the backscattering intensity is mainly affected by the surface roughness and moisture content of agricultural field. The substantial

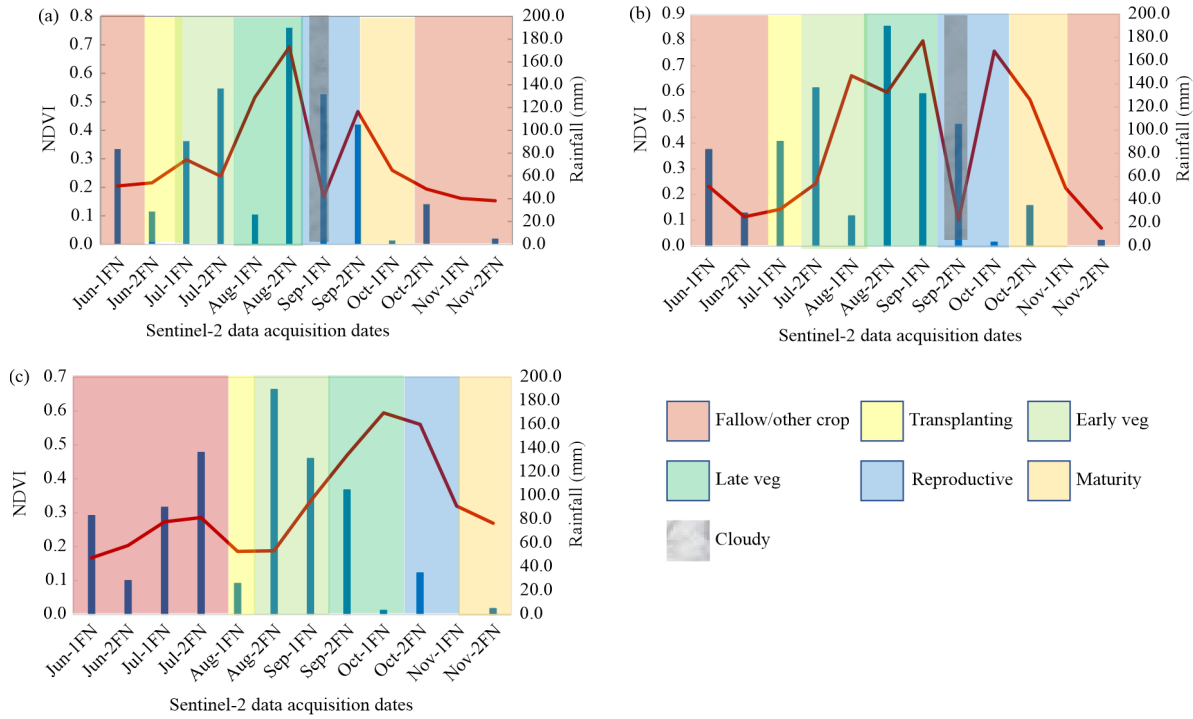


Fig. 5. Temporal NDVI profiles of paddy crop representing (a) early rice, (b) normal rice, and (c) late rice

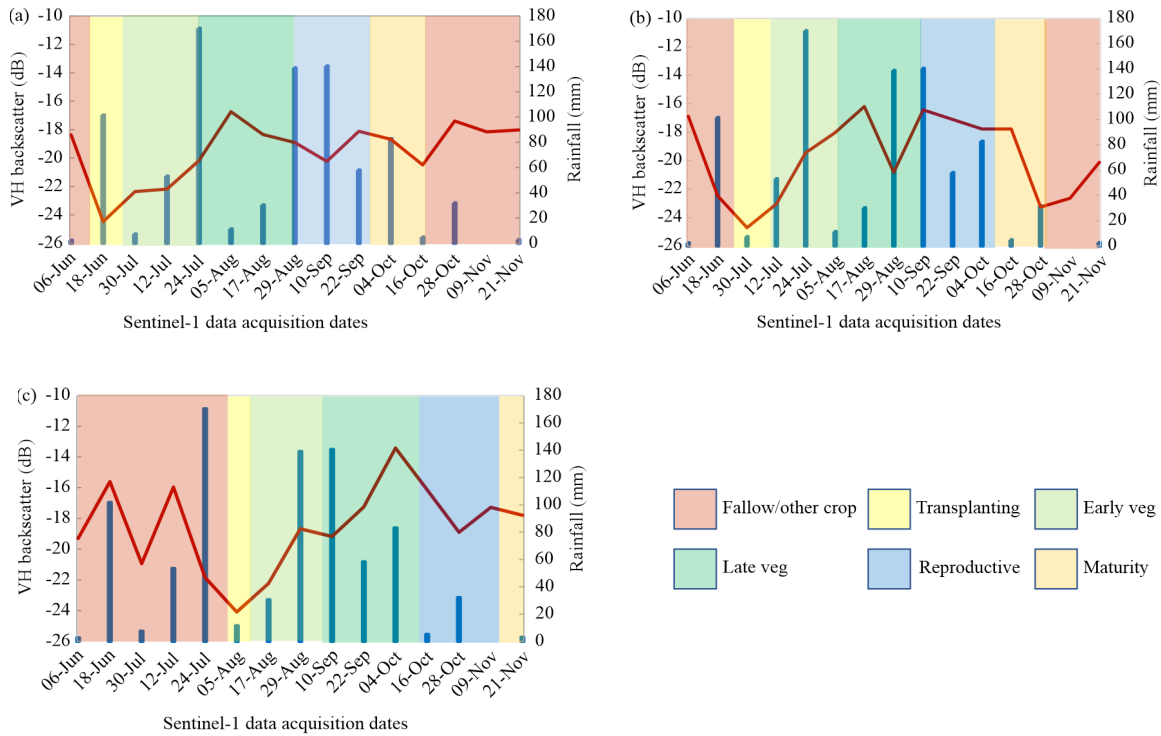


Fig. 6. Temporal VH backscatter profiles of paddy crop representing (a) early rice, (b) normal rice, and (c) late rice

dip in backscattering at transplanting stage was due to the flooded field conditions as the smooth water surface shows low backscattering values (Phung *et al.*, 2020; Son *et al.*, 2018). The increase in backscatter intensity at tillering stage could be inferred as a result of germination and tillers development, and drying of the underlying ground surface, which caused double-bounce reflections emerged from the interaction between paddy vegetation and ground surface. Then at the late vegetation stage and till the reproductive stage increase in the backscatter intensity was as expected to result from the increase in number of tillers, growth of leaves, stem elongation, flowering, and grain formation. At the maturity stage till harvest stage, the decreasing trend of backscatter values might have been as a result of plant dryness and therefore reduction in the homogeneity of crop at maturity towards harvest stage.

Characteristics of SAR observables and NDVI with respect to paddy phenological growth stages

The box and whisker plots (Fig. 7) showed the backscattering intensities in co-polarization VV, cross-polarization VH, RVI, ratio VH/VV, VV+VH, VV-VH, VV-VH/VV+VH and NDVI at different phenological growth stages. In the current study, response of all the observables was analysed from transplanting to harvesting.

At the transplanting stage, the VH backscatter intensity ranged from the greatest value of -22.5 dB to the least value of -27.0 dB, with the median value being -24.5 dB. It then rised at the early vegetative stage, when the median value is -19.0 dB. The median value of -16.7 dB indicates that the trend was still upwards till the late vegetative stage. After that, the trend toward reproductive and maturity stage continuously declined.

The backscattering intensity of VV was characterized by an increasing trend till late vegetative stage, with median values -14.5 dB at transplanting stage to -11.0 dB at late vegetative stage. Similar to the VH backscattering intensity, VV backscatter intensity also decreased during the reproductive and maturity stages but it was not as significant as VH backscattering. The median value

of VV backscattering was -11.1 dB during reproductive stage and diminished to -11.4 dB at maturity stage. Similar results were seen in the studies of Salsabila *et al.* (2021) for assessing the paddy phenological stages and observed that VV backscatter ranged between -16 to -5 and VH backscatter ranged between -24 to -13 for paddy.

The ratio VH/VV also initiated with an increasing trend with median values -11.5 dB at transplanting stage and continues to increase significantly till late vegetative stage (median value is -5.0dB). Following that, VH/VV exhibited a gradually decreasing trend between -5.8 dB to -6.5 dB during the reproductive and maturity stage. Similarly, Kobayashi and Ide (2022) monitored the paddy phenological stages using VH/VV and reported the similar results.

The response of RVI was comparable to the backscatter intensities mentioned above. During transplanting and late vegetative stage, it had a rising trend, going from a median value of 0.3 to 0.8. Then, as the plant reaches maturity, it dropped to 0.6.

The sum VV+VH and subtraction VV-VH showed sensitivity towards transplanting, early vegetative and maturity stages. The SAR observables VV+VH and VV-VH exhibited insignificant patterns for late vegetative and reproductive stages. Beginning with the modest decline from transplanting to early vegetative stage, the normalised ratio VV-VH/VV+VH continued to decline throughout the late vegetative stage. It showed a slight increase as it approached maturity stage.

At the transplanting stage, the water background with small plant height and less canopy coverage attributed to the very low observable values. Therefore, the values of all observables at this stage were significantly lower from the other growth stages which credited to the decent discrimination accuracy (Table 3). On the other hand, the ranges of all observables overlapped with each other for vegetative and reproductive growth stages for rice. During these periods, the canopy coverage over the water background increased continuously due to increased plant height and density. Moreover, increase in the plant elements (leaves, stem elongation and panicles) has exhibited the ambiguous change in the observables, regardless of change in

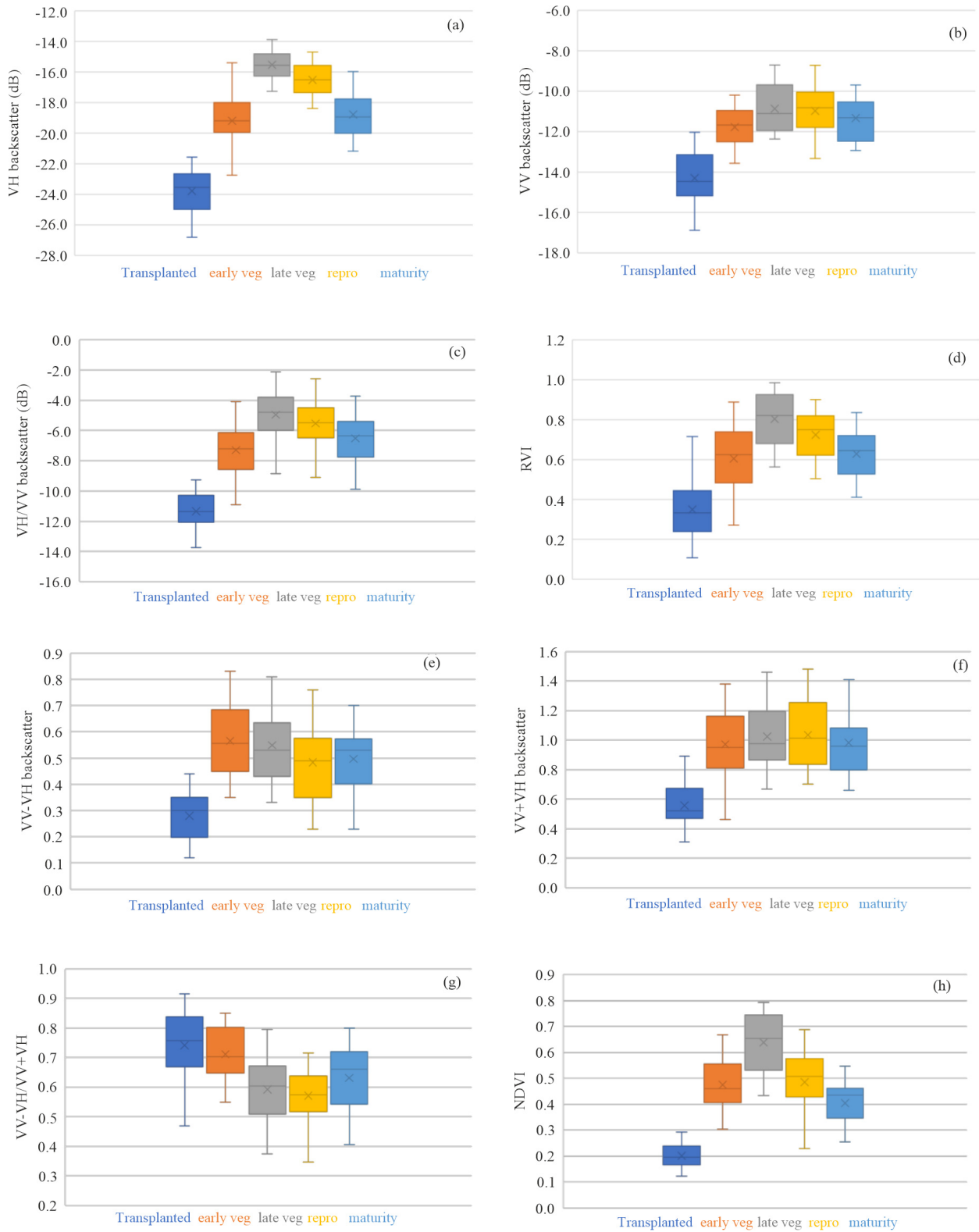


Fig. 7. Backscattering of (a) VH (dB) , (b) VV (dB), (c) VH/VV (dB), (d) RVI, (e) VV-VH, (f) VV+VH, (g) VV-VH/VV+VH, and (h) NDVI at different phenological stages of paddy

the plant geometry. However, the changes in observables were affected by slow changes in canopy moisture (Kobayashi and Ide, 2022; Umutoiwase and Lee, 2021; Supriatna *et al.*, 2019; Verma *et al.*, 2019), evident during maturity phase. In November month, rice crop was at full senescence stage or about to be harvested, with negligible canopy moisture, led to decrease in values of all observables. The pattern of the VH and VV for different paddy phenological stages was found to be in accordance with the studies of Umutoiwase and Lee (2021) and Verma *et al.* (2019).

Of all the SAR-based observables, VH, VH/VV and RVI showed consistent patterns to all the paddy phenological stages. Additionally, NDVI showed same trend as VH backscattering, but only few cloud free pixels were available. It was observed that none of the single SAR observables alone could discriminate phenological growth stages for the entire growth period. However, the combined use of selected SAR observables can help to attain the discrimination of growth stages with desired accuracy. Therefore, rule-based classification using four observables was carried out to extract the spatial phenological growth stage.

Rules development and rice phenology retrieval

In the current study, a rule-based classification was selected for three reasons: (a) to develop the basic understanding by coupling knowledge of rice crop phenology and the information content of SAR data, (b) to select the threshold based on observed temporal

differences and changes, and apply progressively to produce a classification, and (c) full control of user for the refinement of rules, at any point in the classification process.

For simplicity, the four selected SAR observables (VH backscatter, VV backscatter, RVI and ratio (VH/VV)) were used to frame the rules to define all the phenological stages for rice crop. The selected threshold to define decision space is depicted by 2-D planes using (a) VH backscatter vs VV backscatter and (b) RVI vs ratio (VH/VV), illustrated in Fig. 8. VH and VV plot (Fig. 8a) demonstrates that a portion of transplanted stage and a portion of the early vegetative stage are overlapped. Even the early vegetative stage and late vegetative, reproductive and harvest stages overlap to some extent. Additionally in VH/VV and RVI plot (Fig. 8b) there was overlapping between transplanting stage and harvesting stage.

The following pre-defined thresholds are used in the study:

- Transplanting stage: $s^0VH < -22$ dB; $s^0VV < -12$ dB; $RVI < 0.4$; and $ratio < -9$ dB
- Early vegetative growth stage: -22 dB $< s^0VH < -17$ dB; -12 dB $< s^0VV < -10$ dB; $0.4 < RVI < 0.7$; and -9 dB $< ratio < -4$ dB
- Advanced vegetative growth stage: $s^0VH > -17$ dB; $s^0VV > -11$ dB; $RVI > 0.7$; and $ratio > -6$ dB
- Reproductive growth stage: -18 dB $> s^0VH > -15$ dB; -12 dB $< s^0VV < -10$ dB; $RVI > 0.6$; and $ratio > -7$ dB

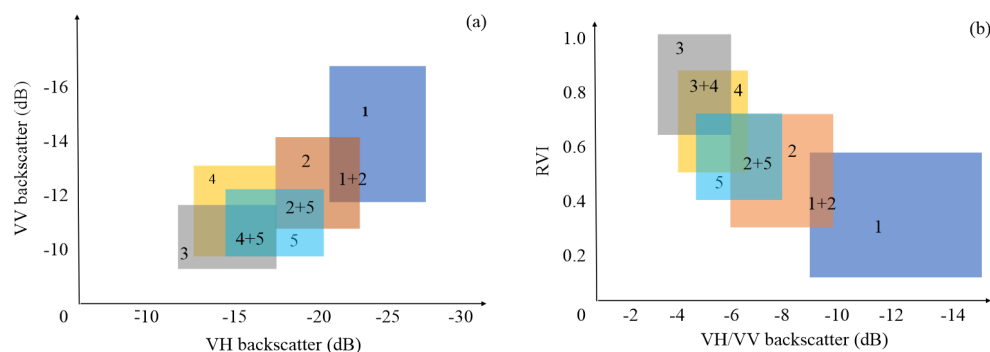


Fig. 8. Intersection of different phenological stages for (a) VV and VH, (b) RVI and ratio (VH/VV). Color coding: dark blue-transplanted stage (1), orange-early vegetative stage (2), grey-late vegetative stage (3), yellow-reproductive stage (4), light blue-maturity (5)

Table 2. Pixel count of paddy growth stage at Sentinel-1 acquisition date

| Acquisition date | Transplanted (%) | Early vegetative (%) | Advanced vegetative (%) | Reproductive (%) | Maturity harvested (%) |
|------------------|------------------|----------------------|-------------------------|------------------|------------------------|
| 06 Jun | 51 | 8 | 7 | 2 | 32 |
| 18 Jun | 67 | 10 | 5 | 3 | 15 |
| 30 Jun | 82 | 12 | 4 | - | 2 |
| 12 Jul | 75 | 21 | 4 | - | - |
| 24 Jul | 41 | 29 | 17 | 8 | 5 |
| 05 Aug | 37 | 36 | 12 | 9 | 6 |
| 17 Aug | 25 | 31 | 30 | 11 | 3 |
| 29 Aug | 15 | 28 | 31 | 22 | 4 |
| 10 Sep | 14 | 26 | 27 | 29 | 4 |
| 22 Sep | 11 | 19 | 32 | 31 | 7 |
| 04 Oct | 7 | 15 | 28 | 42 | 8 |
| 16 Oct | 4 | 12 | 29 | 38 | 17 |
| 28 Oct | - | 16 | 26 | 33 | 25 |
| 09 Nov | - | 24 | 15 | 18 | 43 |
| 21 Nov | - | 26 | 17 | 18 | 39 |

(e) Maturity / harvested stage: $-22 \text{ dB} < s^0 \text{VH} < -17 \text{ dB}$; $-12 \text{ dB} < s^0 \text{VV} < -10 \text{ dB}$; $0.4 < \text{RVI} < 0.8$; and $-7 \text{ dB} < \text{ratio} < -3 \text{ dB}$

Firstly, the four SAR variables extracted from field points were divided in the ratio of 70:30 for analysis and validation, respectively. Then, for the retrieval of paddy phenology, above rules were applied using selected SAR variables at pixel level at all dates. Only few field points were available for a particular phenological stage on the particular date of satellite acquisition. The progression of phenology with each date was traced agreeably with respect to ground data at the same date. In the study area, due to variability of rice transplanting time within the same rice type led to variation in the onset of forthcoming growth stages. This was captured well in the retrieved phenology and illustrated as the percentage of pixels corresponding to a particular growth stage at each acquisition date, given in Table 2. It was observed that most of the pixels matched to the dominant growth stage or transition stages as per the ground data. However, there was some undesirable mixing during assigning the growth stages (e.g., pixels at early vegetative growth stage during maturity stage) due to classification error which may be accounted to the overlapped signature due to complex scattering mechanism and inherent

noise in SAR data.

The performance of rule-based classification to retrieve phenology was evaluated for its accuracy using the remaining 30% of ground observed phenology (validation points) and the confusion matrix table is given in Table 3. The overall accuracy was 68.42% with kappa statistics of 0.59. The user's accuracy was between 60% and 76.92%. The producer's accuracy was between 46.15% and 100%.

Conclusions

The current study presented the opportunity of Sentinel-1 SAR based observables and Sentinel-2 derived NDVI to analyse the paddy phenological stages in the Nizamabad district of Telangana, India. The results indicated that NDVI profile is affected by cloud and so that SAR data was used over optical data for temporal profile analysis of paddy. Temporal VH backscatter and NDVI profiles could characterise the staggered transplanting periods of paddy and sensitivity of SAR backscattering coefficients and NDVI to paddy phenological stages were explored. The SAR observables have shown the distinct temporal behaviour in response to different phenological stages of paddy with some overlaps. Majority of the SAR based observables such as, VH

Table 3. Confusion matrix showing classification accuracies of paddy stages

| Classification Results (pixels) | Ground reference data (pixels) | | | | | | | User's accuracy (%) | Producer's accuracy (%) |
|---------------------------------------|--------------------------------|--------------------------|-------------------------|-------------------|----------|-----------|-------|---------------------------|-------------------------------|
| | Trans- planted | Early vege- tative | Late vege- tative | Repro- ductive | Maturity | Harvested | Total | | |
| Transplanted | 10 | 0 | 0 | 0 | 0 | 3 | 13 | 76.92 | 100.00 |
| Early vegetative | 0 | 32 | 3 | 3 | 3 | 2 | 43 | 74.41 | 76.19 |
| Late vegetative | 0 | 6 | 23 | 6 | 3 | 0 | 38 | 60.52 | 74.19 |
| Reproductive | 0 | 3 | 3 | 18 | 2 | 0 | 26 | 69.23 | 58.06 |
| Maturity | 0 | 1 | 1 | 3 | 15 | 2 | 22 | 68.18 | 60.00 |
| Harvested | 0 | 0 | 1 | 1 | 2 | 6 | 10 | 60.00 | 46.12 |
| Total | 10 | 42 | 31 | 31 | 25 | 13 | 152 | | |

Overall accuracy = 68.42%; Kappa statistics = 0.59

backscatter, VV backscatter, RVI, ratio VH/VV showed sensitivity to paddy growth stages, however, VV-VH and VV+VH backscattering. It was observed that none of the single SAR observables alone could discriminate phenological growth stages for the entire growth period. Therefore, combined use of selected SAR observables discriminated the growth stages with a accuracy of 68.42%.

Acknowledgement

Authors thank the NRSC, Hyderabad, India; and WTC, PJTSAU, Hyderabad for providing constant encouragement and facility to carry out the work.

References

- Ali, A.M., Savin, I., Poddubskiy, A., Abouelghar, M., Saleh, N., Abutaleb, K., El-Shirbeny, M. and Dokukin, P. 2021. Integrated method for rice cultivation monitoring using Sentinel-2 data and Leaf Area Index. *The Egyptian Journal of Remote Sensing and Space Science* **24**(3): 431-441.
- Amin, E., Belda, S., Pipia, L., Szantoi, Z., El Baroudy, A., Moreno, J. and Verrelst, J. 2022. Multi-Season phenology mapping of Nile Delta croplands using time series of Sentinel-2 and Landsat 8 green LAI. *Remote Sensing* **14**(8): 1812.
- Bouvet, A., Le Toan, T. and Lam-Dao, N. 2009. Monitoring of the rice cropping system in the Mekong Delta using ENVISAT/ASAR dual polarization data. *IEEE Transactions on Geoscience and Remote Sensing* **47**(2): 517-526.
- Chakraborty, M., Manjunath, K.R., Panigrahy, S., Kundu, N. and Parihar, J.S. 2005. Rice crop parameter retrieval using multi-temporal, multi-incidence angle Radarsat SAR data. *ISPRS Journal of Photogrammetry and Remote Sensing* **59**(5): 310-322.
- De Castro, A.I., Six, J., Plant, R.E. and Pena, J.M. 2018. Mapping crop calendar events and phenology-related metrics at the parcel level by object-based image analysis (OBIA) of MODIS-NDVI time-series: A case study in central California. *Remote Sensing* **10**(11): 1745.
- Dong, J. and Xiao, X. 2016. Evolution of regional to global paddy rice mapping methods: A review. *ISPRS Journal of Photogrammetry and Remote Sensing* **119**: 214-227.
- Elert, E. 2014. Rice by the numbers: A good grain. *Nature* **514**(7524): S50-S50.
- FAOSTAT. 2021. Production/Yield Quantities of Rice, Paddy in World. Food and Agriculture Organization of the United Nations.
- Harfenmeister, K., Itzerott, S., Weltzien, C. and Spengler, D. 2021. Detecting phenological development of winter wheat and winter barley using time series of Sentinel-1 and Sentinel-2. *Remote Sensing* **13**(24): 5036.
- Hisham, N.H.B., Hashim, N., Saraf, N.M. and Talib, N. 2022, July. Monitoring of Rice Growth Phases Using Multi-Temporal Sentinel-2 Satellite Image. In *IOP Conference Series: Earth and Environmental Science*.

- Htitiou, A., Boudhar, A., Lebrini, Y., Hadria, R., Lionboui, H. and Benabdelouahab, T. 2022. A comparative analysis of different phenological information retrieved from Sentinel-2 time series images to improve crop classification: A machine learning approach. *Geocarto International* **37**(5): 1426-1449.
- Kobayashi, S. and Ide, H. 2022. Rice Crop Monitoring Using Sentinel-1 SAR Data: A Case Study in Saku, Japan. *Remote Sensing* **14**(14): 3254.
- Le Toan, T., Ribbes, F., Wang, L.F., Floury, N., Ding, K.H., Kong, J.A., Fujita, M. and Kurosu, T. 1997. Rice crop mapping and monitoring using ERS-1 data based on experiment and modeling results. *IEEE Transactions on Geoscience and Remote Sensing* **35**(1): 41-56.
- Li, R., Xu, M., Chen, Z., Gao, B., Cai, J., Shen, F., He, X., Zhuang, Y. and Chen, D. 2021. Phenology-based classification of crop species and rotation types using fused MODIS and Landsat data: The comparison of a random-forest-based model and a decision-rule-based model. *Soil and Tillage Research* **206**: 104838.
- Lin, W., Zhang, F.C., Jing, Y.S., Jiang, X.D., Yang, S.B. and Han, X.M. 2014. Multi-temporal detection of rice phenological stages using canopy spectrum. *Rice Science* **21**(2): 108-115.
- Lopez-Sanchez, J.M., Cloude, S.R. and Ballester-Berman, J.D. 2011. Rice phenology monitoring by means of SAR polarimetry at X-band. *IEEE Transactions on Geoscience and Remote Sensing* **50**(7): 2695-2709.
- Lopez-Sanchez, J.M., Vicente-Guijalba, F., Ballester-Berman, J.D. and Cloude, S.R. 2013. Polarimetric response of rice fields at C-band: Analysis and phenology retrieval. *IEEE Transactions on Geoscience and Remote Sensing* **52**(5): 2977-2993.
- Low, J., Ullmann, T. and Conrad, C. 2021. The impact of phenological developments on interferometric and polarimetric crop signatures derived from Sentinel-1: Examples from the DEMMIN Study Site (Germany). *Remote Sensing* **13**(15): 2951.
- Meier U. 1997. BBCH-monograph. In Growth Stages of Plants. *Blackwell* 622.
- Moran, M.S., Alonso, L., Moreno, J.F., Mateo, M.P.C., De La Cruz, D.F. and Montoro, A., 2011. A RADARSAT-2 quad-polarized time series for monitoring crop and soil conditions in Barrax, Spain. *IEEE Transactions on Geoscience and Remote Sensing* **50**(4): 1057-1070.
- Onojeghuo, A.O., Blackburn, G.A., Wang, Q., Atkinson, P.M., Kindred, D. and Miao, Y. 2018. Rice crop phenology mapping at high spatial and temporal resolution using downscaled MODIS time-series. *GI Science and Remote Sensing* **55**(5): 659-677.
- Pandit, A., Sawant, S., Mohite, J. and Pappula, S. 2021. Sentinel-1-derived coherence time-series for crop monitoring in Indian agriculture region. *Geocarto International* 1-21.
- Phung, H.P., Nguyen, L.D., Nguyen-Huy, T., Le-Toan, T. and Apan, A.A. 2020. Monitoring rice growth status in the Mekong Delta, Vietnam using multitemporal Sentinel-1 data. *Journal of Applied Remote Sensing* **14**(1): 014518.
- Pipia, L., Belda, S., Franch, B. and Verrelst, J. 2022. Trends in satellite sensors and image time series processing methods for crop phenology monitoring. In *Information and Communication Technologies for Agriculture—Theme I: Sensors*. 199-231.
- Shao, Y., Fan, X., Liu, H., Xiao, J., Ross, S., Brisco, B., Brown, R. and Staples, G. 2001. Rice monitoring and production estimation using multitemporal RADARSAT. *Remote sensing of Environment* **76**(3): 310-325.
- Salsabila, C., Ghazali, M.F. and Zaenudin, A. 2021. Historical paddy rice growth and phenology pattern estimation using dual polarization of Sentinel 1. In *2021 7th Asia-Pacific Conference on Synthetic Aperture Radar*. 1-5.
- Sisheber, B., Marshall, M., Ayalew, D. and Nelson, A. 2022. Tracking crop phenology in a highly dynamic landscape with knowledge-based Landsat–MODIS data fusion. *International Journal of Applied Earth Observation and Geoinformation* **106**: 102670.
- Son, N.T., Chen, C.F., Chen, C.R. and Minh, V.Q. 2018. Assessment of Sentinel-1A data for rice crop classification using random forests and support vector machines. *Geo carto International* **33**(6): 587-601.
- Supriatna, R., Wibowo, A., Shidiq, I.P.A., Pratama, G.P. and Gandharum, L. 2019. Spatio-temporal analysis of rice field phenology using Sentinel-1

- image in Karawang reGENCY West Java, Indonesia. *International Journal* (62): 101-106.
- Umutohiwase, N. and Lee, S.K. 2021. The Potential of Sentinel-1 SAR Parameters in Monitoring Rice Paddy Phenological Stages in Gimhae, South Korea. *Korean Journal of Remote Sensing* **37**(4): 789-802.
- United Nations. 2017. The sustainable development goals report.
- USDA 2021-22. World Rice Production.
- Verma, A., Kumar, A. and Lal, K. 2019. Kharif crop characterization using combination of SAR and MSI Optical Sentinel Satellite datasets. *Journal of Earth System Science* **128**(8): 1-13.
- Wang, M., Wang, J., Chen, L. and Du, Z. 2022. Mapping paddy rice and rice phenology with Sentinel-1 SAR time series using a unified dynamic programming framework. *Open Geosciences* **14**(1): 414-428.
- Wang, Y., Fang, S., Zhao, L., Huang, X. and Jiang, X. 2022. Parcel-based summer maize mapping and phenology estimation combined using Sentinel-2 and time series Sentinel-1 data. *International Journal of Applied Earth Observation and Geoinformation* **108**: 102720.
- Wu, F., Wang, C., Zhang, H., Zhang, B. and Tang, Y. 2010. Rice crop monitoring in South China with RADARSAT-2 quad-polarization SAR data. *IEEE Geoscience and Remote Sensing Letters* **8**(2): 196-200.
- Zhao, W., Qu, Y., Zhang, L. and Li, K. 2022. Spatial-aware SAR-optical time-series deep integration for crop phenology tracking. *Remote Sensing of Environment* **276**: 113046.

Received: 6 August 2022; Accepted: 24 September 2022